JOURNAL OF SOLID STATE CHEMISTRY 72, 363–375 (1988)

Structure, Ionic Conductivity, and Phase Transformation in New Polymorphs of the Double Chloride Spinel, Li_2FeCl_4

R. KANNO,* Y. TAKEDA, A. TAKAHASHI, AND O. YAMAMOTO

Department of Chemistry, Faculty of Engineering, Mie University, Tsu, 514 Japan

AND R. SUYAMA† AND S. KUME

College of General Education, Osaka University, Osaka, 560 Japan

Received February 4, 1987; in revised form May 19, 1987

A new low-temperature modification of Li_2FeCl_4 was prepared by annealing the metastable cubic spinel at 100°C for 2 weeks. It was characterized by Rietveld X-ray structure refinement, differential thermal analysis, high-temperature X-ray diffraction analysis, and electrical conductivity measurement. The new phase has *Imma* symmetry with lattice parameters $a = 7.3067(3)$, $b = 7.3158(4)$, and $c = 10.3323(5)$ Å; its orthorhombic (o) unit cell is related to that of the cubic spinel (c) according to $a_o \sim \frac{1}{2}^{1/2}a_c$, $b_o \sim \frac{1}{2}^{1/2}a_c$, and $c_o \sim a_c$. The orthorhombic distortion is caused by a 1 : 1 ordering of Li^+ and Fe^{2+} ions on the octahedral sites. Stoichiometric orthorhombic Li_2FeCl_4 decomposed at 126°C to the non-stoichiometric cubic spinel $Li_{2-2x}Fe_{1+x}Cl_4$ and the new Suzuki-type phase Li_6FeCl_8. Stoichiometric cubic Li_2FeCl_4, which is stable above 450°C, was quenched to ambient temperature. Electrical conductivity measurements on the orthorhombic modification and the metastable cubic spinel proved that the distorted structure has the lower ionic conduction. The conduction mechanism in both structures is discussed.

Introduction

The spinel system $Li_{2-2x}M_{1+x}X_4$ (M = Mg, V, Mn, Fe, Cd; X = Cl, Br) has attracted considerable interest not only because of its high ionic conductivity, particularly apparent at moderate temperature, but also because of the transition from a low to a high ionic conducting state exhibited by gradual displacement of lithium ions (*1–8*). The chloride spinels are reported to have the inverse spinel structure in which half of the lithium ions are tetrahedrally surrounded by chloride ions and the other half, together with the M^{2+} ions, are distributed statistically over the octahedral sites (*6, 9*). The chloride spinels have a high ionic conductivity of around 0.1 S cm^{-1} at 400°C. The conductivity values at elevated temperatures are similar to or greater than those for the high lithium ion conductors reported previously (*10*).

As a part of our work on halide spinels, we reported previously the ionic conductivity and the phase transition from a low to a

* To whom correspondence should be addressed.

† Present address: Shinnippon Steel Corporation, Central R & D Bureau, R & D Laboratories-1, Materials Research Lab.-1, Kawasaki, Japan.

0022-4596/88 $3.00

high conducting state of the iron spinel $Li_{2-2x}Fe_{1+x}Cl_4$ (*3*). The iron spinel has the inverse spinel structure and its Arrhenius conductivity plots show a smooth change in slope at a high temperature. The break in conductivity corresponds to a transition from a low to a high conducting state, the precise nature of which has been discussed in detail in the context of the structure and thermodynamics of $Li_{2-2x}M_{1+x}Cl_4$ (M = Mg, Mn) systems (*6, 8*). The transition low to high ionic conduction only was observed in the iron spinel system, while in the magnesium and manganese systems, a transition to a defective NaCl-type structure was found at a higher temperature.

X-ray diffractograms of the iron spinel stored for an extended period at room temperature in an evacuated tube revealed many broad extra reflections not apparent in previous studies and not accounted for by the cubic inverse spinel structure. They could be caused either by decomposition to an unknown phase or by a transition to a low-temperature modification. Mössbauer spectroscopy data (*11*) of this stored sample were inconsistent with the model expected from the inverse cubic spinel structure, random distribution of the iron and lithium ions in the octahedral sites.

We recently found a new distorted orthorhombic cobalt spinel, Li_2CoCl_4 (*12*). The orthorhombic lattice, caused by a 1 : 1 ordering of the Li^+ and Co^{2+} ions on the octahedral sites, transformed to the cubic spinel structure at 308°C and the transition in the cation distribution over the octahedral sites was of the order–disorder type. The X-ray diffraction pattern of the orthorhombic lattice was characterized both by additional weak reflections, such as $(002)_o$, $(020)_o$, and $(200)_o$, and by line splittings in most of the main reflections such that the cubic $(400)_c$ line was split into the orthorhombic $(220)_o$ and $(004)_o$ lines with an intensity ratio of 2 : 1. (The suffixes c and o stand for the cubic and orthorhombic structures, respectively.) The extra X-ray peaks of the stored iron spinel were similar and suggested that the new iron spinel formed at room temperature over an extended period and might have a structure closely related to that of the cobalt spinel.

The purpose of this investigation is to obtain more insight into the iron spinel. We first assumed, and later were able to prove, the existence of a low-temperature iron spinel modification. The structure of the new low-temperature modification was determined by X-ray powder Rietveld analysis. The ionic conductivity of both the orthorhombic and cubic spinels was examined and compared. The phase diagram near the spinel formation domain was also studied.

Experimental

Anhydrous lithium chloride, iron dichloride, and cobalt dichloride were used (LiCl: Nakarai Co., >99% purity; $CoCl_2$: Nakarai Co., >99% purity; $FeCl_2$: Alfa Products). Reactants were dried carefully under vacuum (~1 Pa) at 300°C; their melting points were in good agreement with reported values. The appropriate quantities of reactants were ground together, pressed into a pellet at 60 MPa in a nitrogen-filled glove box, and heated in an evacuated Pyrex tube at 400°C for 1 week. X-ray diffraction patterns of the powdered samples were obtained with both monochromated Cu$K\alpha$ and Cu$K\beta$ radiation and a scintillation detector. A high-power X-ray powder diffractometer (Rigaku RAD, 12 kW) was also used to detect intermediate compounds. A 7-μm-thick aluminum window covered the sample holder to prevent moisture attack during the measurement.

X-ray powder diffraction data for Rietveld analysis were collected on the polycrystalline sample of Li_2FeCl_4 with Cu$K\alpha$ radiation by means of a high-power X-ray powder diffractometer equipped with a

graphite monochromator. The sample was kept under He during measurement. Diffraction data were collected by step scanning over an angular range of $10° < 2\theta < 100°$ in increments of 0.02° at room temperature.

The structural refinement of X-ray data was performed with the Rietveld analysis computer program RIETAN provided by H. Izumi (*13*). Reflection positions and intensities were calculated for both $CuK\alpha_1$ (λ = 1.5405 Å) and $CuK\alpha_2$ (λ = 1.5443 Å) with a factor of 0.5 applied to the latter's calculated integrated intensities. A pseudo-Voigt profile function was used; the mixing parameter γ was included in the least-squares refinement.

The high-temperature phases were examined with a high-temperature X-ray diffractometer. Diffraction patterns were taken in a dry nitrogen atmosphere with silicon powder as the internal standard. Differential thermal analysis (DTA) was carried out for samples sealed in evacuated silica glass containers with α-Al_2O_3 as a standard. Heating and cooling rates were 1.5°C/min.

Electrical conductivities of ~0.5-g pressed pellets were measured in the temperature range between room temperature and 500°C in a dry argon gas flow. Blocking electrodes were deposited on both sides of the pellets by evaporating gold. The conductivity was obtained by ac impedance measurement with a HP4800A vector impedance meter over a frequency range of 5 Hz–500 kHz. Resistances were derived by interpretation of the complex impedance plane diagram of the data.

The oxidation number of the iron ions in both reactants and products was determined to be 2.00 by chemical analysis using iodometry (*14*), an indication that the samples were devoid of Fe^{3+} ions, which can lead to electronic conductivity. The absence of trivalent iron was also confirmed by the Mössbauer effect; these data will be published elsewhere (*11*).

Results and Discussion

1. Synthesis and Structure Refinement

X-ray diffractograms of the iron spinel Li_2FeCl_4 stored for several years showed a number of broad extra lines, e.g., d = 5.20 and 3.67 Å, that were not observed in the previous studies. The pattern was similar to that of the cobalt spinel. The extra reflections could be indexed roughly by the same cubic spinel lattice with reflections d = 5.20 and 3.67 Å indexed as (200) and (220), respectively. However, some reflections such as (200) are inconsistent with the extinction requirements of the cubic spinel space group ($Fd3m$). The distortion of the iron spinel was apparently small since $(400)_c$ and $(440)_c$ reflections were not split. The orthorhombic distortion in the cobalt spinel is caused by a 1 : 1 ordering of the Li^+ and Co^{2+} ions on the octahedral B sites such that more than 80% of lithium ions are arranged along the b axis and the cobalt ions are arranged along the a axis. Since the extra lines in the stored iron spinel are due to a modification that arises at ambient temperature, reflection broadness might be dependent on duration of storage or extent of ordering.

It was expected that annealing just below the transition temperature would facilitate equilibrium and enable the monophasic low-temperature modification to be obtained. Therefore, the solid solution Li_2CoCl_4–Li_2FeCl_4 was studied to estimate both the Li_2FeCl_4 transition temperature and the lattice distortion of the iron spinel. The X-ray diffraction measurements on the solid solution revealed a single phase with orthorhombic symmetry in the whole composition range. The line splittings characteristic of the orthorhombic distortion decreased as composition was varied from x = 1 to 0.25 (see Fig. 1). In this figure, the lattice parameters for the composition x = 0 (stoichiometric Li_2FeCl_4) were determined after the specimen had been annealed at

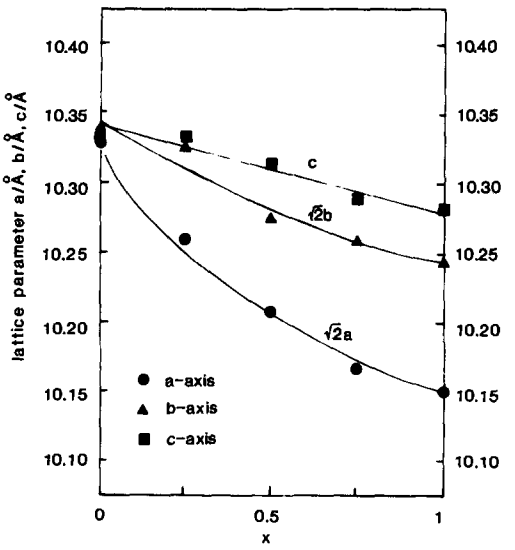

FIG. 1. Lattice parameters in $Li_2(Fe_{1-x}Co_x)Cl_4$ at room temperature. The parameters at $x = 0$ were obtained by the Rietveld method.

100°C as described later. It is apparent that the lattice parameters increase and the distortion decreases as x in $Li_2(Fe_{1-x}Co_x)Cl_4$ approaches 0. The phase transition temperature, determined for the composition range $1 > x > 0.25$ by DTA, is presented in Fig. 2. High-temperature X-ray diffraction data for $x = 0.5$ and 1.0 confirmed that the transition was from orthorhombic to cubic symmetry, consistent with the endothermic DTA peaks at 227 and 308°C, respectively. The transition temperature in the solid solution decreases with increasing iron content x and is estimated by extrapolation to be approximately 130°C at $x = 0$ (Li_2FeCl_4), consistent with the observed value for the sample annealed at 100°C, as described in Section 2.

The sample at $x = 0$ after being annealed at 100°C for 2-weeks showed the sharp additional reflections, the intensities of which were much higher than those observed for the stored sample. High-angle reflections taken by Cu$K\beta$ radiation showed line broadening that could also be caused by the same orthorhombic lattice as that of the cobalt spinel. The cell constants are presented in Table I and are plotted in Fig. 1. The orthorhombic cell could be related to the parent cubic spinel as follows:

$$\begin{pmatrix} a_o \\ b_o \\ c_o \end{pmatrix} = \begin{pmatrix} \frac{1}{2} & \frac{1}{2} & 0 \\ -\frac{1}{2} & \frac{1}{2} & 0 \\ 0 & 0 & 1 \end{pmatrix} \begin{pmatrix} a_c \\ b_c \\ c_c \end{pmatrix}.$$

Diffraction extinctions presented in Table I are characteristics of the space groups *Imma* and *Ima*2.

Refinement of the structure proceeded directly with centrosymmetric space group D_{2h}^{28}–*Imma*. The initial coordinates for the model were those described for Li_2CoCl_4 (*12*) (Li(1): 8i (x, 0.25, z) $x = \frac{1}{8}$, $z = \frac{1}{4}$; Li(2): 4b; Co: 4d; Cl(1): 8h (0, y, z) $y = 0$, $Z = \frac{1}{4}$; Cl(2): 8i $x = \frac{1}{4}$, $z = 0$). A partial disorder of the Li^+ and Fe^{2+} ions on the 4b and 4d octahedral sites was also taken into account. The refinement was done in stages, with the atomic coordinates, thermal parameters, and disordering factor held fixed in the initial calculations and subsequently allowed to vary only after the scale, background,

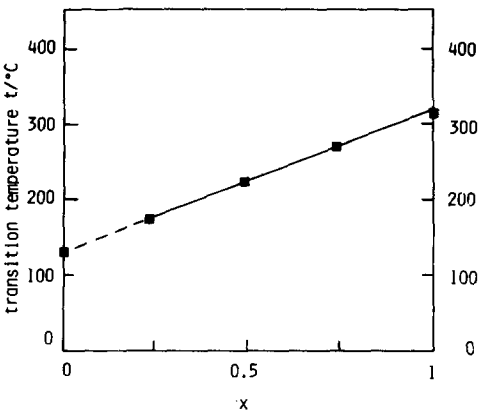

FIG. 2. Thermal evolution of transition temperatures in $Li_2(Fe_{1-x}Co_x)Cl_4$. The transition temperature at $x = 0$ was determined from a sample annealed at 100°C for 2 weeks.

TABLE I

RIETVELD REFINEMENT RESULTS FOR Li_2FeCl_4

Space group	D_{2h}^{28} – *Imma*
Diffraction extinctions	$khl: h + k + l = 2n$
	$kh0: h = 2n$ and $k = 2n$
	$0kl: k + l = 2n$
	$h0l: h = 2n$ and $l = 2n$
	$h00: h = 2n$
	$0k0: k = 2n$
	$00l: l = 2n$
No. of variables	29
Scale factor	0.00988(4)[a]
FWHM parameter U	0.246(17)
V	−4.577(11)
W	0.048(2)
Asymmetry parameter	0.356(23)
Gaussian fraction	0.301(8)
FWHM (Gauss)/FWHM (Lorentz)	2.43(5)
Lattice constant a (Å)	7.3067(3)
b (Å)	7.3158(4)
c (Å)	10.3323(5)

Fractional coordinates

Atom	Site	Occupancy	x	y	z	B (Å^2)
Li(1)	8i	0.5	0.146(15)	0.25	0.196(13)	0.3(31)
Li(2)	4b	0.880(13)	0	0	0.5	3.4(11)
Fe(1)	4b	0.120	0	0	0.5	3.4
Fe(2)	4d	0.880	0.25	0.25	0.75	0.8(1)
Li(3)	4d	0.120	0.25	0.25	0.75	0.8
Cl(1)	8h	1	0	−0.015(3)	0.245(3)	1.4(1)
Cl(2)	8i	1	0.251(6)	0.25	−0.005(3)	2.0(1)

[a] The esd's in parentheses refer to the last significant digit.

half-width, and unit cell parameters were close to their optimum values. Refinement proceeded smoothly to yield agreement factors $R_{wp} = 14.45\%$, $R_p = 10.88\%$, and $R_B = 5.51\%$, with an expected agreement $R_E = 4.73\%$, where wp is the weighted profile, p is the profile, and B is the Bragg intensity. The observed and calculated X-ray diffraction powder profiles are compared in Fig. 3. Table I shows the final structural parameters for Li_2FeCl_4. The interatomic distances and bond angles are listed in Table II.

The structure of the low-temperature modification of Li_2FeCl_4 is derived basically from the inverse spinel structure, which consists of a cubic close-packed anion array with cations occupying, in an ordered manner, one-eighth of the tetrahedral A sites and one-half of the octahedral B sites. The structure, shown in Fig. 4, is ordered with the Fe^{2+} and half of the Li^+ ions occupying the B sites. About 90% of lithium ions that occupy the B sites and are located in position 4b lie along the b axis, and 90% of the iron ions located in position 4d lie along the a axis. The $FeCl_6$ octahedra are connected along the a axis by sharing Cl(1)–Cl(1) edges. Because of the mutual

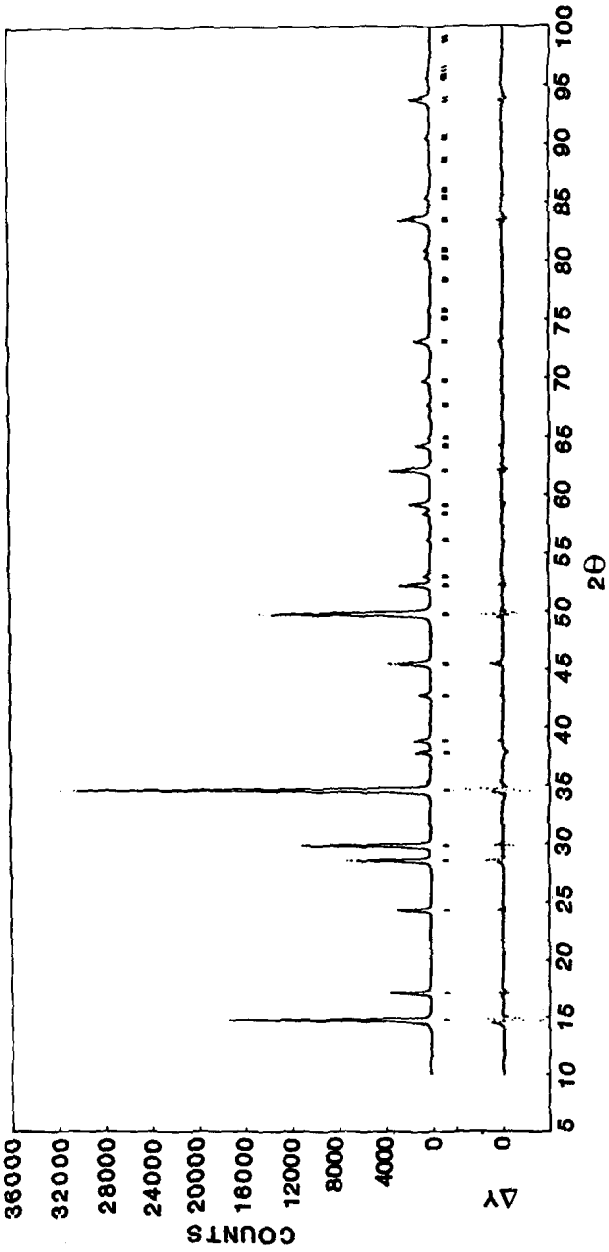

FIG. 3. Observed, calculated, and difference plots of Li_2FeCl_4 X-ray data.

TABLE II

BOND LENGTHS AND ANGLES FOR Li_2FeCl_4

I. Lithium(1)–cholorine	Distance or angle (Å or degree)
Li(1)–Cl(1) (×2)	2.27(6)[a]
Li(1)–Cl(1) (×2)	3.28(9)
Li(1)–Cl(2) (×2)	2.22(13)
Li(1)–Cl(2) (×2)	3.27(14)
Li(1)–Li(1)	2.13(15)
Li(1)–Li(1)	1.87(16)
Li(1)–Li(1)–Li(1)	143(9)
II. Lithium(2)–chlorine	
Li(2)–Cl(1) (×2)	2.57(3)
Li(2)–Cl(2) (×4)	2.63(4)
Cl(1)–Li(2)–Cl(2) (×4)	87.05(78)
Cl(1)–Li(2)–Cl(2) (×4)	92.95(78)
Cl(2)–Li(2)–Cl(2) (×2)	90.5(11)
Cl(2)–Li(2)–Cl(2) (×2)	89.5(11)
Cl(1)–Li(2)–Cl(1) (×2)	180
Cl(2)–Li(2)–Cl(2)	180
III. Iron–chlorine	
Fe(1)–Cl(1) (×4)	2.52(3)
Fe(1)–Cl(2) (×2)	2.50(1)
Cl(1)–Fe(1)–Cl(1) (×2)	86.4(5)
Cl(1)–Fe(1)–Cl(1) (×2)	93.5(5)
Cl(1)–Fe(1)–Cl(2) (×4)	89.2(12)
Cl(1)–Fe(1)–Cl(2) (×4)	90.8(12)
Cl(1)–Fe(1)–Cl(1) (×2)	180
Cl(1)–Fe(1)–Cl(2)	180

[a] The esd's presented here are manual estimates derived from the esd's of the atomic coordinates and they therefore merely provide a guide toward the reliability of each value.

repulsion of the M^{2+} ions in a chain of linked octahedra along the *a* axis, one might expect the length of the Fe–Cl(1) bond to be somewhat greater than that of the Fe–Cl(2) bond, but the observed difference is not significant in relation to the estimated standard deviation. The Fe–Cl distances of 2.54 and 2.51 Å are slightly longer than the corresponding distances of 2.489 and 2.480 Å found in the Li_2CoCl_4 structure because the ionic radius of the divalent iron ion (0.92 Å) is larger than that of the cobalt ion (0.885 Å).

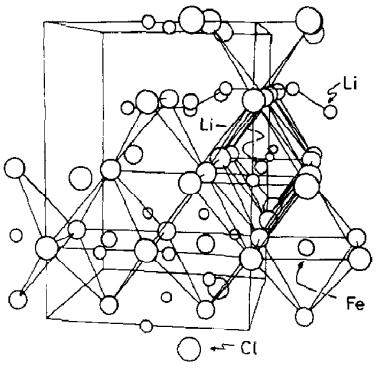

FIG. 4. The structure of Li_2FeCl_4.

The other half of the lithium ions are distributed statistically on the 8*i* sites placed between the 4e tetrahedral (A spinel sites) and 4c interstitial sites. The arrangement of the 4e, 4c, and 8i sites is shown in Fig. 5, and is similar to that found acceptable for Li^+ in Li_2CoCl_4 (*12*). The 8*i* sites lie along the *a* axis.

2. *Thermodynamic Behavior at Elevated Temperatures*

The DTA curves for heated Li_2FeCl_4 showed an endothermic peak at 126°C, in good agreement with the estimated value of 130°C obtained by extrapolation in the $Li_2(Co_xFe_{1-x})Cl_4$ solid solution. On cooling,

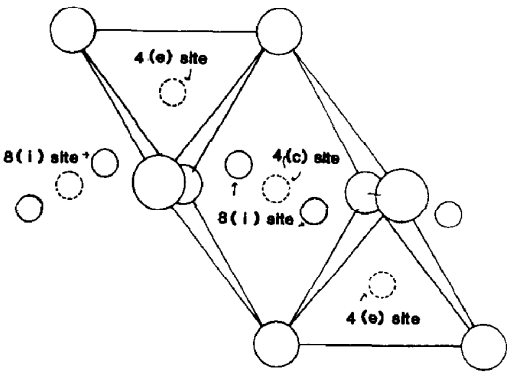

FIG. 5. The arrangement of the 4e, 4c, and 8i sites in Li_2FeCl_4.

however, no heat anomaly is observed around 130°C, an indication that the high-temperature cubic phase is quenched. This is consistent with the X-ray results that the samples prepared by usual methods show the patterns of the cubic spinel structure, while those annealed at 100°C show the orthorhombic structure. The DTA curve on heating shows near 241°C a small endothermic peak, which will be discussed later.

High-temperature X-ray diffraction studies were carried out to elucidate phases that appeared at corresponding temperatures. The orthorhombic $(002)_o$, $(020)_o$, and $(200)_o$ lines disappear between 115 and 180°C. The DTA peak at 126°C definitely corresponds to the phase change from the orthorhombic structure to the cubic spinel structure. The diffraction patterns at 273 and 390°C, on the other hand, indicate the coexistence of two structure types, one the cubic spinel structure and the other a LiCl-type structure. The cubic $(440)_c$ lines at 273 and 390°C split into $(440)_{spinel}$ and $(440)_{LiCl}$ lines. Figure 6 shows the thermal evolution of the lattice parameters of both the cubic spinel and the LiCl-type structure determined from a specimen heated twice. The lattice parameters for the LiCl-type structure are multiplied by 2 to facilitate plotting. On first heating, the parameters of the LiCl-type structure increased steeply from 270 to 390°C, whereas those of the cubic spinel increased gradually from 130 to 390°C. After being cooled to room temperature, the sample showed the diffraction pattern characteristic of the cubic spinel structure. The same sample was then heated again to 450°C. The diffraction patterns on second heating indicated the monophasic cubic spinel structure at all temperatures examined. The lattice parameters of the cubic spinel on the second heating, plotted in Fig. 6, are larger than those on the first heating. The previous X-ray results showed that the lattice parameter of the nonstoichiometric spinel $Li_{2-2x}Fe_{1+x}Cl_4$ decreases linearly with x or with increasing vacancy (*3*). The cubic spinel on first heating therefore apparently contained vacancies that led to lattice parameters smaller than those observed on second heating.

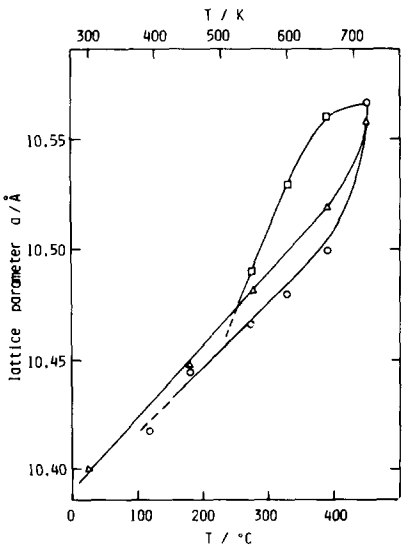

FIG. 6. Thermal evolution of lattice parameters of cubic Li_2FeCl_4 (○, on first heating; △, on second heating) and LiCl solid solution (□).

We investigated the phase diagram of the LiCl–$FeCl_2$ system to clarify the phase relationship near the spinel formation domain. A previous phase study indicated only one intermediate compound, $Li_{2-2x}Fe_{1+x}Cl_4$ (*3*). Our work, however, revealed another new intermediate compound, Li_6FeCl_8. The crystal structure and electrical conductivity of this Suzuki-type Li_6FeCl_8 will be published elsewhere (*15*). Figure 7 shows the phase diagram near the spinel formation domain constructed by DTA and high-temperature X-ray measurements. At room temperature, the system contains two intermediate compounds, the orthorhombic spinel, Li_2FeCl_4, and the Suzuki-type Li_6FeCl_8. At 259°C, the Suzuki-type phase decomposed to the LiCl-type solid solution and the nonstoichiometric cubic spinel $Li_{2-2x}Fe_{1+x}Cl_4$. The stoichiometric Le_2Fe

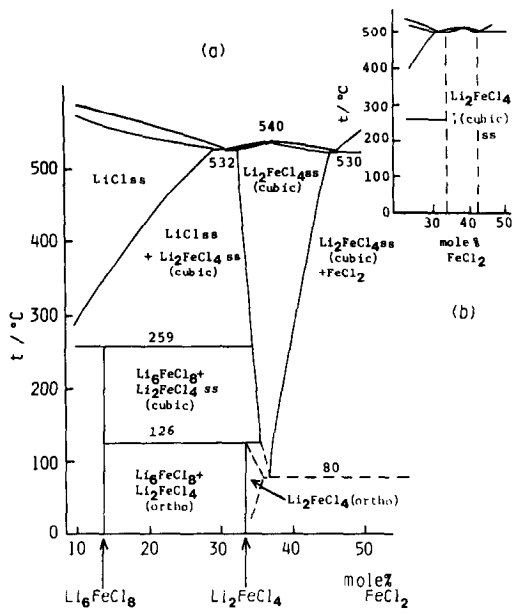

FIG. 7. (a) Phase diagram near the spinel formation domain in the LiCl–$FeCl_2$ system. (b) Phase diagram for the metastable Li_2FeCl_4.

Cl_4 decomposed to $Li_{2-2x}Fe_{1+x}Cl_4$ and Li_6FeCl_8 at 126°C. The stoichiometric Li_2FeCl_4 examined by high-temperature X-ray diffractometry on first heating was actually a mixture of the nonstoichiometric spinel and the LiCl-type solid solution between 273 and 390°C; it became the monophasic cubic spinel above 450°C. The small endothermic DTA peak observed around 241°C was due to the decomposition of the coexisting Suzuki-type phase Li_6FeCl_8. In other words, the stoichiometric sample contains a small amount of Li_6FeCl_8 between 126 and 259°C.

The stoichiometric spinel formed around 450°C could be quenched to ambient temperature even though the cooling rate was relatively low. The X-ray diffraction results for the stoichiometric sample, as described before, showed that on second heating the sample consisted of the monophasic cubic spinel at all temperatures examined. This indicates that the decomposition of the stoichiometric cubic spinel proceeded relatively slowly to the nonstoichiometric spinel and Li_6FeCl_8 or the LiCl-type solid solution, and that the heating and cooling rates during DTA and X-ray diffraction measurements were not low enough to attain equilibrium. Therefore, the experimental results with samples heated to 450°C enable us to construct the nonequilibrium phase diagram shown in Fig. 7b, where the range of solid solution was $0 < x < 0.02$ in $Li_{2-2x}Fe_{1+x}Cl_4$ at room temperature. In a previous paper (*3*), we determined the range of solid solution to be $0.05 < x < 0.2$ using samples cooled slowly after being heated to 400°C. The discrepancy in the range of the solid solution was caused by the difference in heating temperature. Under equilibrium conditions, the solid solution formation limit in $Li_{2-2x}Fe_{1+x}Cl_4$ was in the range $0.05 < x < 0.20$ not at room temperature but at 400°C. The cubic spinel metastable at room temperature, on the other hand, had the composition range $0 < x$ when the sample was quenched from a temperature above 450°C.

The nonstoichiometric cubic spinels with $x = 0.1$ and 0.2 (38 and 43 mol% $FeCl_2$, respectively) decomposed to $FeCl_2$ and the cubic spinel with higher lithium content after being annealed at 100°C. X-ray diffraction analysis of the same samples annealed at 80°C revealed a mixture of the orthorhombic Li_2FeCl_4 and $FeCl_2$. The range of the solid solution for the cubic spinel near 100°C is therefore rather limited, as shown in Fig. 7a.

3. Electrical Properties

The electrical conductivities of the samples measured with ionically blocking electrodes showed a frequency dependence over the temperatures examined. Complex impedance plane analysis enabled us to estimate the bulk resistance. The impedance diagram at room temperature shows a semicircle in the high-frequency range due to a parallel combination of the bulk electrolyte resistance with the bulk capacity. The bulk

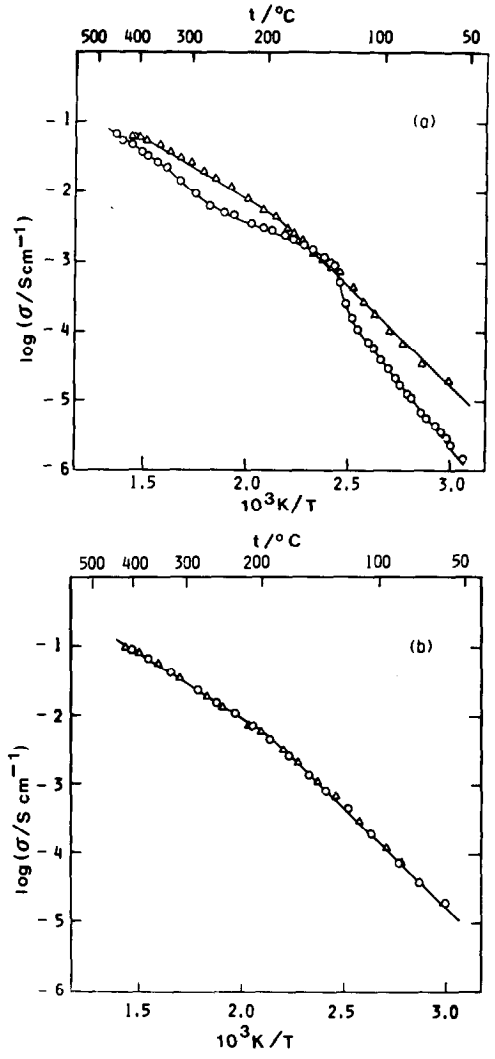

FIG. 8. Temperature dependence of the conductivity for Li_2FeCl_4. (a) Curves on first heating (○) and cooling (△). (b) Curves on second heating (○) and cooling (△).

resistance was obtained by the real-axis intercept of the semicircle at a lower frequency. The impedance diagram at higher temperatures consisted of a straight line, and no semicircle due to bulk capacity was observed. The electrolyte resistances were obtained by extrapolation to the real axis.

Figure 8 shows the Arrhenius plots of the conductivity of Li_2FeCl_4. On first heating, as shown in Fig. 8a, there is a distinct break in the curve around 130°C, corresponding to the lattice's structural change from orthorhombic to cubic. The conductivity curve is complicated between 130 and 500°C, and the conductivity value varies from sample to sample in this temperature range. On cooling, Arrhenius plots showed a smooth change in slope near 200°C. The activation energy increased below the break in the conductivity curve. Figure 8b shows the conductivity curves on second heating and cooling. The conductivities obtained here were exactly the same as those from the first cooling. A change in slope was again observed near 200°C.

The phase relations described previously completely explain the ionic conductivity behavior. The increase in conductivity around 130°C (shown in Fig. 8a) is caused by the phase change from the orthorhombic to the cubic spinel structure. The strange behavior of the conductivity curve between 130 and 450°C on first heating resulted because the sample was a mixture of the spinel and Li_6FeCl_8 or the LiCl-type solid solution. The conductivity rises gradually with temperature between 300 and 500°C, suggesting an increase in the amount of a more highly conductive phase. This is in good agreement with the X-ray results that the amount of the LiCl solid solution decreased and the highly conductive spinel phase increased from 300 to 450°C. The conductivity curve on cooling can be interpreted as that of the monophasic metastable cubic spinel, since X-ray diffractometry revealed that the cubic spinel can be quenched. The X-ray diffraction data taken after the first cycle of the conductivity measurement confirmed the presence of the cubic spinel.

The conductivity curves obtained in the second cycle have the character of the stoichiometric cubic spinel. The change in slope observed around 200°C was considered to be the phase transition from the low

to the high conducting state. However, no heat anomaly corresponding to the change in slope was observed in DTA curves. The transition from the low to the high conducting state was also observed in all Li_2MX_4 specimens between 200 and 300°C. The precise structural and thermodynamic nature of this transition was studied in detail for the $Li_{2-2x}M_{1+x}Cl_4$ (M = Mg, Mn) system. A neutron diffraction study on Li_2MgCl_4, for example, has revealed gradual displacement of lithium ions from the tetrahedral 8a to the interstitial 16c sites (*6*). These two sites are almost equally populated by lithium ions above the curve in the conductivity plot. This evolution occurs without any other significant change in the structure, particularly in the space group $Fd3m$ and for the cation distribution on the 16d octahedral sites. Characteristically, the temperature dependence of the pattern was a gradual decrease in the intensity of odd-numbered reflections such as (111), corresponding to the transition. The thermodynamic measurement using DSC also confirmed the phase transition from the low to the high ionic conducting state for $Li_{2-2x}M_{1+x}Cl_4$ (M = Mg, Mn) (*8*). By analogy with the magnesium spinels, a disordered arrangement of lithium ions over 8a tetrahedral and 16c octahedral interstitial sites is also expected for the iron spinel in the high ionic conducting state. The gradual intensity decrease in X-ray peaks such as (111) is certain evidence of the lithium ion displacement on the iron spinel.

The conductivity data for Li_2FeCl_4 are summarized in Table III. Activation energies are calculated for both high and low conducting states. The conductivity data on first heating below 120°C enable us to calculate the activation energy for the orthorhombic modification. The activation energies of the cubic spinel were calculated for both the low- and high-temperature ranges from the data on second heating. The orthorhombic structure has lower conductivity and higher activation energy than the cubic spinel. Low ionic conduction of distorted structures was previously reported from bromide spinels (Li_2MgBr_4, Li_2MnBr_4) (*7*) and for the cobalt spinel (Li_2CoCl_4) (*11*). The bromide spinels have the orthorhombic (Li_2MgBr_4 (*7*)) and tetragonal (Li_2MnBr_4 (*16*)) structures at room temperature. They were expected to have an activation energy for ionic conduction lower than that of the chloride spinels because the bromide ion is more highly polarizable than the chloride ion. However, the conductivity measurement clarified higher activation energies than the corresponding chloride spinels, an indication that the ionic conduction was seriously affected by the lattice distortion. For chloride spinels, the orthorhombic Li_2CoCl_4 also had an activation energy higher than that of other cubic chloride spinels. The difference in ionic conduction between the cubic and distorted structures was clearly observed for the iron spinel, because two modifications exist in the same temperature range from room temperature to 126°C. Lower lithium ion conduction in the distorted modification was then confirmed, as shown in Table III.

TABLE III

ACTIVATION ENERGY FOR IONIC CONDUCTION IN Li_2FeCl_4

Structure	Activation energy E (kJ mole^{-1})	
	Low-temperature range	High-temperature range
Cubic structure	56	39
Orthorhombic structure	73	

Lower ionic conduction may be explained tentatively on the basis of the structural results. In the cubic spinel structure, lithium ions on the A sites participate in

ionic conduction, and the conduction path is three-dimensional along the 8a tetrahedral–16c interstitial octahedral–8a tetrahedral sites (*6*). Our structural results on Li_2FeCl_4, on the other hand, suggest that ionic conduction in Li_2FeCl_4 is likely due to the motion of lithium ions in the 8i sites and that the diffusion pathway is directed only along the *a* axis of the orthorhombic lattice. Furthermore, the 8i positions are situated in the octahedron, which is the interstitial site for the cubic spinel structure, as shown in Fig. 5. The differences in both the conduction path and the position of the lithium ions explain the lower ionic conduction of the orthorhombic modification.

Summary

A new room-temperature modification of the iron spinel, Li_2FeCl_4, was obtained by annealing the cubic spinel at 100°C for 2 weeks. The structure was refined by the X-ray Rietveld method using the spinel, Li_2CoCl_4, as a model. The orthorhombic distortion is caused by the 1 : 1 ordering of cations over the octahedral B sites, with about 90% of lithium and iron ions arranged along the *b* and *a* axes, respectively.

The spinel's thermodynamic behavior was investigated by DTA and high-temperature X-ray analysis. Stoichiometric orthorhombic Li_2FeCl_4 decomposed at 126°C to the nonstoichiometric cubic spinel $Li_{2-2x}Fe_{1+x}Cl_4$ and Suzuki-type Li_6FeCl_8, which was recently found to exist up to 259°C. Stoichiometric cubic Li_2FeCl_4 can be quenched from above 450°C to yield a range of solid solution of $0 < x$ for the metastable cubic spinel, $Li_{2-2x}Fe_{1+x}Cl_4$.

Ionic conductivity was measured for both the new orthorhombic modification and the metastable cubic spinel. The distorted modification had lower ionic conduction, probably because of differences both in dimensionality of the conduction path and in the position of the lithium ions. Arrhenius conductivity plots of the cubic iron spinel showed a smooth change in slope around 200°C. The break in conductivity curves corresponded to the transition from the low to the high conducting states, caused by gradual displacement of lithium ions over the tetrahedral 8a and the interstitial octahedral 16c sites.

Acknowledgments

Reflection intensity measurements were performed at the Materials Analyzing Center at the Institute of Scientific and Industrial Research, Osaka University. We thank Mr. Tanaka of the Center for his assistance in the measurements. All computations for the structure refinement were carried out at the Crystallographic Research Center, Institute of Protein Research, Osaka University. We thank Professors K. Kamiya and T. Yoko at Mie University for the use of a high-temperature X-ray diffractometer and Professor M. Takano for useful discussions.

References

1. R. Kanno, Y. Takeda, and O. Yamamoto, *Mat. Res. Bull.* **16,** 999 (1981).
2. H. D. Lutz, W. Schmidt, and H. Haeuseler, *J. Phys. Chem. Solids* **42,** 287 (1981).
3. R. Kanno, Y. Takeda, and O. Yamamoto, *Solid State Ionics* **9 & 10,** 153 (1983).
4. C. Cros, L. Hanebali, L. Latie, G. Villeneuve, and G. Wang, *Solid State Ionics* **9 & 10,** 139 (1983).
5. R. Kanno, Y. Takeda, K. Takada, and O. Yamamoto, *J. Electrochem. Soc.* **131,** 469 (1984).
6. J. L. Soubeyroux, C. Cros, G. Wang, R. Kanno, and M. Pouchard, *Solid State Ionics* **15,** 293 (1985).
7. R. Kanno, Y. Takeda, O. Yamamoto, C. Cros, G. Wang, and P. Hagenmuller, *J. Electrochem. Soc.* **133,** 1053 (1986).
8. R. Kanno, Y. Takeda, O. Yamamoto, C. Cros, G. Wang, and P. Hagenmuller, *Solid State Ionics* **20,** 99 (1986).
9. C. J. J. van Loon and J. de Jong, *Acta Crystallogr. Sect.* **B 31,** 2549 (1975).
10. P. Hagenmuller and W. van Gool (Eds.), "Solid Electrolytes," Academic Press, New York (1978).

11. R. KANNO, Y. TAKEDA, O. YAMAMOTO, AND M. TAKANO, to be published.

12. R. KANNO, Y. TAKEDA, A. TAKAHASHI, O. YAMAMOTO, R. SUYAMA, AND S. KUME, *J. Solid State Chem.* **71,** 1 (1987).

13. F. IZUMI, *J. Mineral Soc. Japan* **17,** 37 (1985) [in Japanese].

14. BUNSEKI KAGAKU BINRAN, p. 98, Maruzen, Tokyo (1981).

15. R. KANNO, Y. TAKEDA, M. MORI, AND O. YAMAMOTO, *Chem. Lett.*, 1465 (1987).

16. W. SCHMIDT AND H. D. LUTZ, *Ber. Bunsenges. Phys. Chem.* **88,** 720 (1984).